RAPID COMMUNICATIONS

PHYSICAL REVIEW A **73**, 020702(R) (2006)

Collisional deexcitation in a quasi-two-dimensional degenerate bosonic gas

I. B. Spielman,[1,*] P. R. Johnson,[1] J. H. Huckans,[1,2] C. D. Fertig,[1,2,†] S. L. Rolston,[1,2] W. D. Phillips,[1,2] and J. V. Porto[1]
[1]*National Institute of Standards and Technology, Gaithersburg, Maryland 20899, USA*
[2]*University of Maryland, College Park, Maryland 20742, USA*

(Received 3 September 2005; published 15 February 2006)

We separate a Bose-Einstein condensate into an array of two-dimensional (2D) sheets and excite quantized vibrational motion in the direction normal to the sheets. The measured collisional decay rates are suppressed due to the reduced dimensionality, a matter wave analog to inhibited spontaneous emission. After decay, the large excitation energy is transferred to back-to-back outgoing atoms, imaged as rings in the 2D plane. The ring diameters correspond to vibrational energy level differences, and edge-on imaging allows identification of the final vibrational states.

DOI: 10.1103/PhysRevA.73.020702 PACS number(s): 34.30.+h, 03.75.Kk, 05.30.Jp

Most quasi-2D quantum systems have been realized with electrons in semiconductors, where a 1D potential confines the electrons to the lowest quantized vibrational states in one direction, i.e., the energies in the 2D plane are much smaller than the vibrational level spacing. Recently it has become possible to confine degenerate atomic Bose gases to 2D [1,2] and investigate vibrational excitations in the tightly confined direction [3]. Trapped 2D atomic gases provide experimental opportunities unavailable in electron systems. For example, unlike semiconductors, the atomic system is nearly defect-free. Further, the dynamic control of the confining potential, coupled with an ability to image the atoms, enables the direct detection of the excited-state population and the momentum distribution. Quantized vibrational states are an ingredient in proposals to realize exotic states of matter, such as striped or super-solid phases [4–6], and are possible motional qubit states for quantum computation [7–9]. Stronger confinement (beyond that described herein) can also change the nature of collisions [10–12].

Here we study the vibrational relaxation of a quasi-2D Bose-Einstein condensate (BEC), where quantized motion in the tightly confined direction plays a role analogous to an internal degree of freedom. We transfer a large fraction of atoms into excited vibrational states, creating highly non-equilibrium atom populations. In this system, atom-atom collisions provide the only significant relaxation mechanism, transferring "internal" energy to 2D kinetic energy. We directly observe atom populations as outgoing rings (Fig. 1) representing distinct decay channels. The excited-state lifetimes are enhanced due to the reduction in the density of final scattering states, relative to scattering into a 3D continuum—analogous to suppressed spontaneous emission in a planar cavity [13]. Scattering in unconfined geometries has been studied, for example, in the context of cold coherent collisions between 3D BECs [14,15].

We create independent 2D sheets (or pancakes) of atoms by applying a deep 1D optical lattice to a 3D BEC. In the tight direction ($\hat{z}$) the system is well-described by a single-particle 1D Schrödinger equation, yielding discrete vibrational levels labeled by an index n. Atoms, Raman-excited from the ground state $n=0$ to $n=1$ or 2, collide and decay. By imaging after a time of flight t_{TOF}, we identify the momentum and population of atoms in the various final vibrational states. We extract excited-state lifetimes from time sequences of these single-shot vibrational spectra.

We produce a magnetically trapped ^{87}Rb BEC with up to 2.5×10^5 atoms in the $|F=1,m_F=-1\rangle$ state [16]. The BEC is separated into a stack of about 80 pancakes by

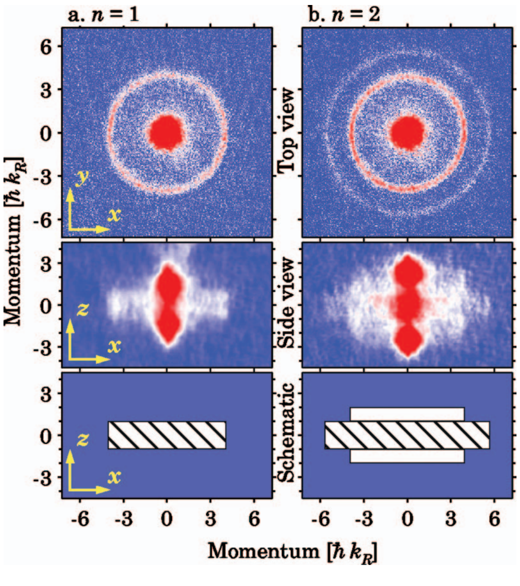

FIG. 1. (Color) Absorption images of vibrationally excited atoms after a 1 ms decay and subsequent TOF, with 60% initial population in the (a) $n=1$ and (b) $n=2$ vibrational levels. In the top views, outgoing rings ($t_{\mathrm{TOF}}=7.1$ ms) correspond to different in-plane energies imparted to the atoms from various decay channels. Viewed from the side ($t_{\mathrm{TOF}}=13.1$ ms) the vertical momentum distribution identifies the vibrational states. Here, the rings appear as rectangles, and the schematic of the side view shows the expected distributions from the dominant decay processes to $n=1$ (white rectangles) and $n=0$ (hatched rectangles). The uncollided fraction in the center of the image (not shown in the schematic) is distributed vertically in accordance with the remaining excited fraction.

---

[*] Electronic address: ian.spielman@nist.gov

[†] Present address: University of Georgia, Athens, GA 30602.

1050-2947/2006/73(2)/020702(4)/$23.00

an optical lattice with period $d=410(1)$ nm [22] vertically aligned along $\hat{z}$ [23]. When in the ground vibrational state, the largest pancake has $N \approx 4.6(10) \times 10^3$ atoms with a chemical potential $\mu=1.6(2)$ kHz; the resulting peak 2D and 3D densities are $2.2(2) \times 10^9$ cm^{-2} and $2.9(3) \times 10^{14}$ cm^{-3}, respectively. The 2D Thomas-Fermi radii are $R_x=11.0(6)$ μm and $R_y=12.0(7)$ μm. In the combined magnetic and optical potential, the in-plane oscillation frequencies are $\omega_x/2\pi=55(1)$ Hz and $\omega_y/2\pi=50(1)$ Hz. The lattice is raised continuously from zero in 200 ms with an exponentially increasing ramp (50 ms time constant). This time scale is chosen to be adiabatic with respect to mean-field interactions and vibrational excitations. By pulsing the lattice and observing the resulting atom diffraction [17], we measure a lattice depth of $s=77(4)$, expressed in units of $E_R=h^2/8md^2=h \times 3.42(2)$ kHz. For a single well of the deep sinusoidal potential, the energy spacings are $E_{n+1}-E_n \simeq E_R[2\sqrt{s}-(n+1)]$ (these energies, which include the lowest-order anharmonic correction, are shifted at the 1% level by the interatomic interaction). The harmonic frequency is $\omega_z/2\pi=2E_R\sqrt{s}/h=60(1)$ kHz.

Raman transitions between vibrational levels [18] are driven by a pair of laser beams. The nearly counterpropagating Raman beams are oriented approximately along $\hat{z}$ [24], are detuned 82 GHz below the ^{87}Rb $D2$ transition, and have a relative detuning δ ranging from 50 to 120 kHz. A 1 ms Raman pulse excites a fraction f_n of the atom population to either $n=1$ or 2.

The anharmonicity of the potential allows us to selectively transfer populations between desired vibrational levels, provided the pulse duration t_p is long enough that its Fourier spread resolves the $\gtrsim E_R/h$ difference from unwanted transitions. t_p must also be shorter than the vibrational lifetime τ. For our experiment (where $\tau \gtrsim t_p \gtrsim \hbar/E_R$), we find that by detuning below Raman resonance and chirping 15 kHz through resonance in 1 ms, we controllably transfer up to 65% of the atoms to either $n=1$ or 2 (simulations indicate a maximum transfer of around 75% in this situation) with only ~5% population in unwanted states [25].

The vibrationally excited atoms are allowed to decay for variable hold times t_{hold} ranging from 10 μs to 10 ms; then the lattice is turned off in 200 μs. The magnetic trap is then turned off in ≈ 300 μs, and the atom cloud expands for t_{TOF} before absorption imaging. The resulting atomic distribution, which constitutes an average over the ~80 pancakes, is imaged along one of two axes: perpendicular to the pancakes (top view, along $\hat{z}$) and edge-on (side view, along $\hat{y}$).

The decay of a pair of atoms from initial vibrational states a and b to final states c and d (denoted $ab \rightarrow cd$) can be viewed as a 2D two-body inelastic collision process, where vibrational states in the confined direction play the role of internal states. The release of vibrational energy leads to back-to-back atom pairs with large momenta in the 2D plane. Figure 1 shows example TOF images from which we can infer the final momentum distribution. Image coordinates are in units of recoil momentum, $\hbar k_R=\pi\hbar/d$ [26], and the corresponding recoil velocity is $\hbar k_R/m=5.6$ mm/s. Each image pair [Figs. 1(a) and 1(b)] contains nearly full spectral information of an excited state and its decay paths.

TABLE I. Release energies (including the lowest-order anharmonic corrections) and matrix elements for the experimentally relevant decay paths and lattice depth $s=77$ (sorted in order of increasing decay energy). The energies denote the per atom difference between initial and final vibrational energies.

Ring	Decay path	E_f-E_i	I_{cd}^{ab}
Central ring	$11 \rightarrow 20$	$E_R/2$	0.0243
	$22 \rightarrow 31$	$E_R/2$	0.0257
	$22 \rightarrow 40$	$2E_R$	0.0007
Inner ring	$11 \rightarrow 00$	$\hbar\omega_z-E_R$	0.2202
	$22 \rightarrow 11$	$\hbar\omega_z-2E_R$	0.1556
	$22 \rightarrow 20$	$\hbar\omega_z-3E_R/2$	0.0020
	$20 \rightarrow 00$	$\hbar\omega_z-3E_R/2$	0.1128
Outer ring	$22 \rightarrow 00$	$2\hbar\omega_z-3E_R$	0.1075

The decay paths allowed by parity and conservation of energy are shown in Table I. For atoms excited to $n=1$, only two decay paths contribute. The high-energy process, $11 \rightarrow 00$, gives rise to the ring in Fig. 1(a) (top view), while the ring from the low-energy $11 \rightarrow 20$ process is not resolved from the central cloud. Each ring's radius corresponds to the atomic in-plane velocity and hence the per atom difference between initial and final vibrational energies. In Fig. 1(b), atoms excited to $n=2$ decay through several channels. The processes $22 \rightarrow 11$, $20 \rightarrow 00$, and $22 \rightarrow 20$ all contribute to the inner ring of Fig. 1(b), each with an energy of about $2E_R\sqrt{s}$ per atom. The outer ring results solely from the $22 \rightarrow 00$ decay process.

Figures 2(a) and 2(b) show the radial density of the atomic cloud after an angular integration of the data in Figs. 1(a) and 1(b), respectively. We extract the vibrational energy spacings by fitting the data to Lorentzians. We attribute the atom background between the peaks to secondary scattering involving outgoing atoms and include it in the fits as a linearly sloping baseline. The measured energies agree with

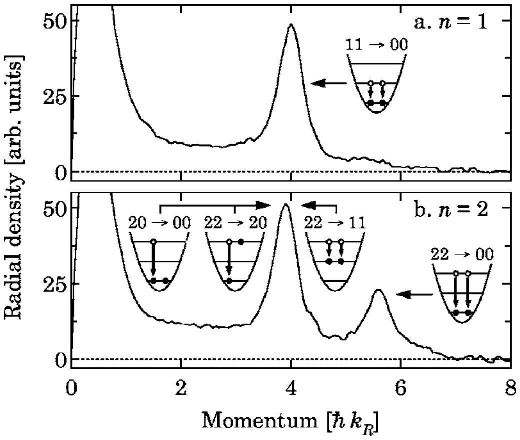

FIG. 2. Angular integrals of top view data. (a) From Fig. 1(a), the single ring gives rise to a peak located at $k=4.0(1)$ k_R. (b) The two rings in Fig. 1(b) yield two peaks at $k=3.9(1)k_R$ and $5.6(2)k_R$. The diagrams schematically illustrate the decay channels which contribute to each peak.

those expected from the known lattice depth, within our 4% experimental uncertainty. The branching ratio between the inner and outer rings estimated from Fig. 2 (ignoring the atom background) is 2.1(3). The value calculated from the matrix elements in Table I is 2.9(3) for an excited fraction $f_2=0.60(5)$.

The side view images in Figs. 1(a) and 1(b) complement the top view images by identifying the final vibrational states. The 200 μs lattice turn-off is adiabatic with respect to the 55 kHz vibrational frequency. As a result, the turn-off procedure maps quasimomentum states in the 1D lattice to the corresponding free-particle momentum states [19,20]. For example, atoms in the $n=1$ vibrational state reside in the second Brillouin zone (BZ), and are mapped to a continuum of momentum states k_z where $k_R<|k_z|<2k_R$ [27].

Figure 1(a) shows atoms which were initially excited into $n=1$. In the side view, the atom cloud's extent along $\hat{z}$ reflects the mapping of quasimomentum to momentum, and the extent in the horizontal direction reflects the final in-plane momentum. The ring in the top view appears as a rectangle in the side view [schematically illustrated by the hatched rectangle in Fig. 1(a)]. The dense, vertically aligned double-lobed structure at the center of the side view image is largely due to atoms which have not decayed and remain in the $n=1$ state (second BZ). Figure 1(b) depicts atoms initially in $n=2$. The process $22\rightarrow 00$ gives rise to atoms in the first BZ [hatched rectangle in Fig. 1(b)], while $22\rightarrow 11$ leads to atoms in the second BZ [white rectangles in Fig. 1(b)]. Note that the vertical central structure is taller since it contains atoms remaining in $n=2$ (third BZ).

We calculate short-time two-body branching ratios and decay rates in a single pancake using Fermi's golden rule. Due to the extreme anisotropy of our potential, the initial condensate wave functions can be approximated as a product of single-particle wave functions, $\Psi_i(x,y,z)\approx\psi(x,y)\varphi_{n_i}(z)$. Here $\psi(x,y)$ satisfies an effective 2D Gross-Pitaevskii equation [10] for $n=0$ atoms in the Thomas-Fermi limit; we assume $\psi(x,y)$ remains unchanged during the short duration of the experiment. The $\varphi_{n_i}(z)$ solve the Schrödinger equation for the 1D lattice potential and are nearly harmonic-oscillator wave functions with an extent $\sigma_z=\sqrt{\hbar/m\omega_z}$. The final states $\Psi_f(x,y,z)=\exp[-i(k_x x+k_y y)]\varphi_{n_f}(z)$ are free particles in x and y, which is justified since $\omega_z\gg\omega_{x,y}$. The rate for the scattering process $ab\rightarrow cd$ is $\Gamma^{ab}_{cd}N_aN_b$, with atom populations N_a and N_b, and

$$\Gamma^{ab}_{cd}=2\pi a_s^2\omega_z I^{ab}_{cd}\int \mathrm{d}x\mathrm{d}y|\psi(x,y)|^4, \tag{1}$$

where $I^{ab}_{cd}=2\pi|\sigma_z\int \mathrm{d}z\varphi_a(z)\varphi_b(z)\varphi_c(z)\varphi_d(z)|^2$ is dimensionless (see Table I), and $a_s=5.3$ nm is the s-wave scattering length [21,28]. Parity considerations make $I^{ab}_{cd}=0$ when $a+b+c+d$ is odd. The total rate is a sum over energetically allowed final states c and d.

For atoms excited to $n=1$, the excited fraction $f_1(t)$ is governed by $\dot{f}_1=-2N[\Gamma^{11}_{00}+2\Gamma^{11}_{20}]f_1^2$. Parity considerations forbid the transition $10\rightarrow 00$ but not $20\rightarrow 00$, so as $f_1\rightarrow 0$ the $n=1$ decay rate per atom $\dot{f}_1/f_1\rightarrow 0$, but as $f_2\rightarrow 0$ the corresponding $n=2$ rate is nonzero. For atoms excited to $n=2$, a pair of coupled equations describe the evolution of $f_2(t)$ and $f_0(t)$.

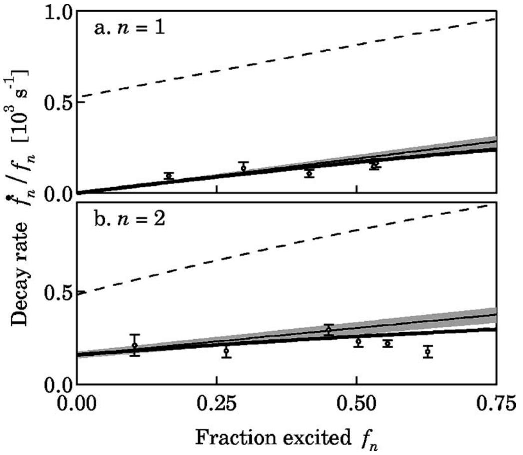

FIG. 3. Initial decay rates. (a) Initial population in $n=1$. (b) Initial population in $n=2$. The thin lines represent the result of our model with no adjustable parameters, integrated over the distribution of pancakes expected from Thomas-Fermi approximation. The gray regions reflect the variation in this model due to experimental number uncertainty. The thick solid lines include the estimated effect of secondary scattering, using a 75% probability of a second event, and the long-dashed lines are the expected decay rate in the absence of 2D confinement.

The excited-state population as a function of t_{hold} is found from a series of side-view images like those in Fig. 1. Integrating over x gives the atomic distribution along $\hat{z}$. To extract populations, we fit the data to a distribution, flat within each BZ, convolved with a Gaussian. The width of the Gaussian is fixed by applying this model to data in which only the ground state (first BZ) was occupied. Repeating the fitting process for different t_{hold} yields the fractional population as a function of time. We extract rates by fitting the first 2 ms to the expected solutions $f_1(t)$ and $f_2(t)$ [29].

The resulting rates per atom at $t=0$ are shown in Fig. 3. For comparison we plot the predicted rates at $t=0$ (thin solid line), where the gray band reflects the experimental atom number uncertainty. The agreement, with no free parameters, is good even though we neglected corrections from secondary collisions. The presence of atoms not on the rings (Figs. 1 and 2) indicates that around 75% atoms rescatter, consistent with our theoretical estimates. These processes decrease the atomic density, and hence reduce the overall decay rate at late times. (In separate experiments with lower density thermal samples, we indeed observe significantly lower rates: below 40 s^{-1}.) The effect should be more significant for large initial excited fractions, a trend consistent with the data. The thick solid lines in Fig. 3 show the estimated effect of secondary scattering from outgoing atoms which decayed during the 1 ms Raman pulse. This lowest-order estimate assumes that each decayed atom can rescatter at most once, and if it does scatter, its secondary-collision partner does not itself rescatter. We suspect that the neglected higher-order collision processes are in part responsible for the excess suppression in Fig. 3(b) for $f>0.5$.

The reduced dimensionality suppresses the total scattering rate in a manner similar to the suppression of spontaneous emission in a planar cavity [13]. A comparison between confined and unconfined decay can be made by considering a situation where the final states of the atomic scattering are unconstrained. For confined final states, the total deexcitation rate $\Gamma_{2\mathrm{D}}$ is given by a discrete sum over energetically allowed final vibrational states, times the (energy-independent) 2D density of in-plane states. For unconfined final states, the total deexcitation rate $\Gamma_{3\mathrm{D}}$ is proportional to the 3D density of final states, which increases as the square root of the scattering energy. Note that, unlike the case of spontaneous emission in a planar cavity, the initial states and energies here are determined by the confining potential, so $\Gamma_{3\mathrm{D}}$ must include the zero-point energies $\hbar\omega_z/2$ of each atom. Figure 3 shows $\Gamma_{3\mathrm{D}}$ (long dashes). For a 100% excited fraction of $n=2$ atoms, $\Gamma_{3\mathrm{D}}/\Gamma_{2\mathrm{D}}\approx 2.4$, and for $n=1$ atoms, $\Gamma_{3\mathrm{D}}/\Gamma_{2\mathrm{D}}\approx 2.9$. In the absence of 2D confinement, the parity restriction which suppressed the decay of $n=1$ atoms as $f\rightarrow 0$ is lifted, so in this case $\Gamma_{3\mathrm{D}}/\Gamma_{2\mathrm{D}}$ diverges [as seen in Fig. 3(a)].

In conclusion, we measured a confinement-induced suppression of the transition rates between different vibrational states in a deep 1D optical lattice using a new, single-shot, spectrographic technique. Additional suppression of the rates would be achieved by further modifying the final density of states [6], for example by confining the atoms into 1D tubes [16], or in analogy with photonic band-gap materials, by applying an additional in-plane lattice to open suitably placed band gaps. The long lifetimes are expected to be useful in the context of producing correlated atomic systems.

We thank E. Tiesinga, P. Naidon, and C. J. Williams for useful conversations. This work was supported in part by ARDA, ONR, and NASA. P.R.J. acknowledges support from the IC research program.

---

[1] A. Görlitz *et al.*, Phys. Rev. Lett. **87**, 130402 (2001).
[2] C. Orzel *et al.*, Science **291**, 2386 (2001).
[3] J. H. Denschlag *et al.*, J. Phys. B **35**, 3095 (2002).
[4] G. Schmid and M. Troyer, Phys. Rev. Lett. **93**, 067003 (2004).
[5] V. W. Scarola and S. D. Sarma, e-print cond-mat/0503378.
[6] A. Isacsson and S. M. Girvin, e-print cond-mat/0506622.
[7] E. Charron, E. Tiesinga, F. Mies, and C. Williams, Phys. Rev. Lett. **88**, 077901 (2002).
[8] K. Eckert *et al.*, Phys. Rev. A **66**, 042317 (2002).
[9] J. V. Porto *et al.*, Philos. Trans. R. Soc. London, Ser. A **361**, 1417 (2003).
[10] D. S. Petrov and G. V. Shlyapnikov, Phys. Rev. A **64**, 012706 (2001).
[11] M. Olshanii, Phys. Rev. Lett. **81**, 938 (1998).
[12] I. Bouchoule, M. Morinaga, C. Salomon, and D. S. Petrov, Phys. Rev. A **65**, 033402 (2002).
[13] R. G. Hulet, E. S. Hilfer, and D. Kleppner, Phys. Rev. Lett. **55**, 2137 (1985).
[14] N. R. Thomas, N. Kjærgaard, P. S. Julienne, and A. C. Wilson, Phys. Rev. Lett. **93**, 173201 (2004).
[15] Ch. Buggle, J. Léonard, W. von Klitzing, and J. T. M. Walraven, Phys. Rev. Lett. **93**, 173202 (2004).
[16] B. L. Tolra *et al.*, Phys. Rev. Lett. **92**, 190401 (2004).
[17] Y. B. Ovchinnikov *et al.*, Phys. Rev. Lett. **83**, 284 (1998).
[18] H. Perrin, A. Kuhn, I. Bouchoule, and C. Salomon, Europhys. Lett. **42**, 395 (1998).
[19] A. Kastberg *et al.*, Phys. Rev. Lett. **74**, 1542 (1995).
[20] H. Stecher *et al.*, Phys. Rev. A **55**, 545 (1997).
[21] E. G. M. van Kempen, S. J. J. M. F. Kokkelmans, D. J. Heinzen, and B. J. Verhaar, Phys. Rev. Lett. **88**, 093201 (2002).
[22] All uncertainties herein reflect the uncorrelated combination of single-sigma statistical and systematic uncertainties. Shot-to-shot fluctuations are the largest source of uncertainty in lattice depth and atom number.
[23] The nearly counterpropagating lattice beams are generated by a Ti:sapphire laser tuned to $\lambda=809.5$ nm, intersecting at $\theta=162(1)^\circ$.
[24] The Raman beams have a $1/e^2$ radius $w_0=1.2$ mm and are canted from $\hat{z}$, leading to a small momentum kick of $0.06k_R$ in the 2D plane.
[25] The Raman chirp is essentially an adiabatic rapid passage. Since the anharmonicity makes the energy spacing $E_{n+1}-E_n$ between consecutive levels decrease as n increases, a down-going chirp is successively resonant with higher transitions, exciting undesired vibrational levels. This is avoided by chirping from below.
[26] After TOF, the atom distribution maps final position to initial momentum. The TOF used in the computation of momentum is increased by 0.5 ms, accounting for the 1 ms window during which the atoms decay.
[27] The 200 ms turn-on procedure is adiabatic with respect to all time scales except inter pancake tunneling. Such a system fills the relevant BZ due to the fact that the essentially random phases develop in different pancakes via spatial variations in mean-field shifts and trapping potentials.
[28] The 3D scattering is largely unaffected by confinement since $a_s=5.3$ nm is much smaller than $\sigma_z\approx 44$ nm [10].
[29] Our model assumes that decayed atoms leave the system forever; in reality the experiment was performed in a ~50 Hz harmonic trap. To assure the validity of our assumptions, we confined our analysis to times much shorter than the trap's 5 ms quarter-period—generally 2 ms. To achieve better signal to noise, we fit the first 5 ms for the $n=1$, $f_1\approx 0.2$ data point.